Electronic Supplementary Material (ESI) for Chemical Communications.

Dealloying-derived nanoporous Sn-doped copper with prior selectivity toward formate for CO_2 electrochemical reduction

Hefeng Yuan *[a], Bohao Kong [b], Zhehao Liu [b], Li Cui [a], Xiaoguang Wang *[b]

[a] Institute of Resources and Environmental Engineering, Shanxi University, Taiyuan 030006, China. E-mail: yuanhefeng@sxu.edu.cn

[b] Laboratory of Advanced Materials and Energy Electrochemistry, College of Materials Science & Engineering, Taiyuan University of Technology, Taiyuan 030024, Shanxi, China. E-mail: wangxiaoguang@tyut.edu.cn

Experimental Methods

Catalyst preparation

To prepare alloying precursor, Al (99.99%), Cu (99.999%) and Sn (99.99%) were used as received from Guantai Metal Materials Co., Ltd. Specifically, the $Al_{88}Cu_xSn_y$ (x+y = 12) ingots were melted in a quartz tube by an arc melting furnace under argon atmosphere for three times. Then, the alloy ingots were subsequently solidified rapidly on copper roller with a speed of 700 rpm by melt-spinning technique to obtain ribbons with 1~2 mm width and ~1.5 μm thick. Afterwards, the as-prepared $Al_{88}Cu_xSn_y$ (x+y = 12) ribbons were chemically dealloyed in 6 M KOH solution at room temperature for 24 h. The resultant nanoporous products were rinsed by deionized water and alcohol in sequential order to remove residual chemicals, and finally dried in vacuum oven at 60℃ for 12 h. According to the feed ratio, the as-prepared nanoporous products are designated as np-Cu, np-$Cu_{11}Sn_1$, np-Cu_1Sn_1 and np-Sn.

Microstructure Characterization

The crystalline phase of the as-prepared samples was characterized by X-ray diffractometer (XRD) on DX-2700 with Cu Kα radiation (λ=1.5406 Å) at 40 kV and 30 mA. The microscopic morphology and chemical composition were examined on a scanning electron microscope (SEM, Gemini-300) equipped with an energy dispersive X-ray (EDX) analyzer. Talos F200X was used to obtain high resolution transmission electron microscope TEM images (HRTEM) and selected area electron diffraction pattern (SAED). The superficial chemical state was investigated by X-ray photoelectron spectroscopy (XPS, ESCALAB 250Xi) with Al Kα radiation at 15 kV and 10 mA.

Electrochemical Measurements

All electrochemical measurements were conducted on a CS2350 (Wuhan Corrtest Instrument Co. Ltd.) electrochemical work station in a two-compartment H-type cell separated by a Nafion 115 membrane, wherein Ag/AgCl and Pt plate

acted as reference electrode and counter electrode, respectively. Both compartments contained 30 mL of the electrolyte (0.1 M $KHCO_3$), which were bubbled with pure CO_2 at a gas flow rate of 20 sccm to obtain CO_2-saturated $KHCO_3$ solution. All measured potentials were converted to the reversible hydrogen electrode (RHE) based on the equation.

$$E_{(vs.\ RHE)} = E_{(vs.\ Ag/AgCl)} + 0.059 \times pH + 0.205.^{1}$$

Products analysis

The gas products were analyzed by gas chromatography (GC-7820, Zhongkehuifen, China), equipped with the flame ionization detector (FID for CO and hydrocarbons) and a thermal conductivity detector (TCD for H_2) with argon as a carrier gas. The Faradic efficiency is calculated as follows:

$$FE = \frac{NV_pC_{st}PF}{V_{st}RTQ_{tot}}$$

N is the number of electrons to form gas molecules (H_2, CO); V_p is the peak area of gas products in GC spectrum; C_{st} is the volume concentration of standard gas; V_{st} is the peak area of standard gas; P is the standard atmospheric pressure (101.3 kPa); F is the Faraday constant (96485 C mol^{-1}); Q_{tot} is the total charge consumed in bulk electrolysis.

The liquid products were quantified by ^1H nuclear magnetic resonance (NMR) (Bruker DRX 400 Advance.), in which 0.5 mL of the electrolyte was mixed with 0.1 mL of heavy water D_2O (D_2O, 99.9 atom% D, Sigma-Aldrich) and dimethyl sulfoxide (DMSO, 99.99%, Sigma-Aldrich) with 56.3 mM as an internal standard. The peak of water was suppressed in the NMR spectra. The FE of the liquid products can be calculated as follows:

$$FE = \frac{NFn}{Q_{tot}}$$

N is the number of electrons to form liquid molecules (N = 2 for $HCOO^-$); F is

the Faraday constant (96485 C mol^{-1}); n is the total molar of liquid products; Q is the total charge consumed in bulk electrolysis.[2]

Density functional theory calculation

All theoretical calculations were performed using the plane-wave software code VASP (Vienna AbInitio Simulation Package) with projector-augmented wave (PAW) pseudopotential.[3] The Perdew–Burke–Ernzerhof (PBE) generalized gradient approximation (GGA) exchange–correlation functional was employed to describe the interactions between core and electrons.[4] Given to the inclusion of long-range dispersion, the semi-empirical dispersion potential correction method described by Grimme (DFT-D3) was applied to correct van der Waals force.[5] The convergence threshold for structural optimization was set as 10^{-5} eV in energy and -0.02 eV in force, respectively. Considering the plane-wave basis restriction, the cutoff energy was set as 400 eV.

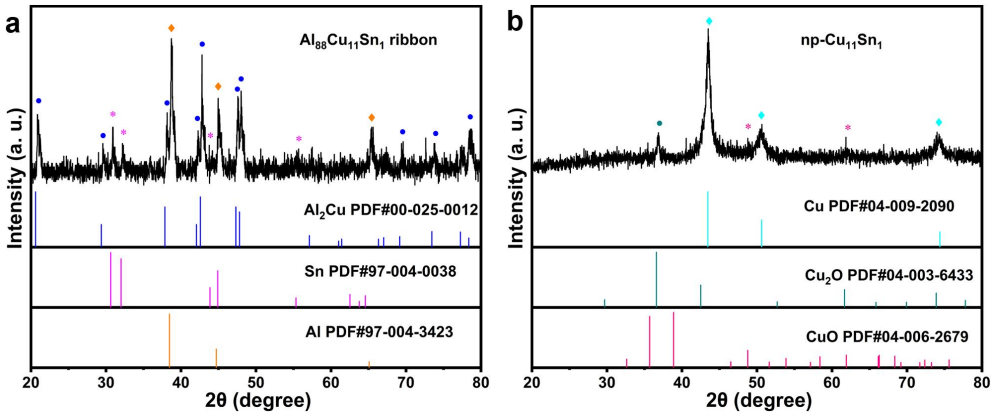

Figure S1. The XRD patterns of $Al_{88}Cu_{11}Sn_1$ and dealloyed np-$Cu_{11}Sn_1$

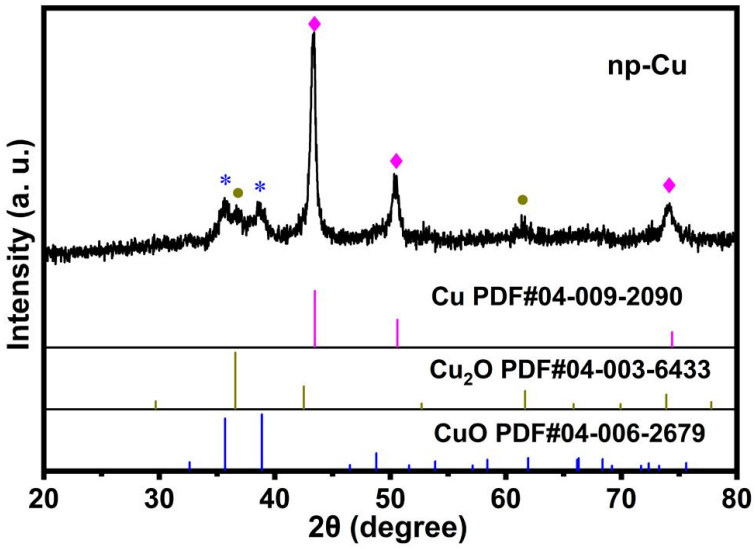

Figure S2. The XRD patterns of np-Cu

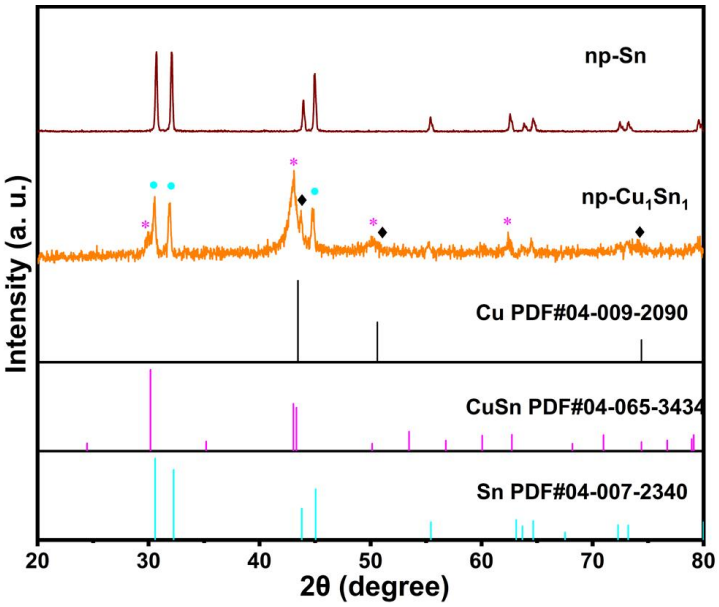

Figure S3. The XRD patterns of np-Cu_1Sn_1 and np-Sn

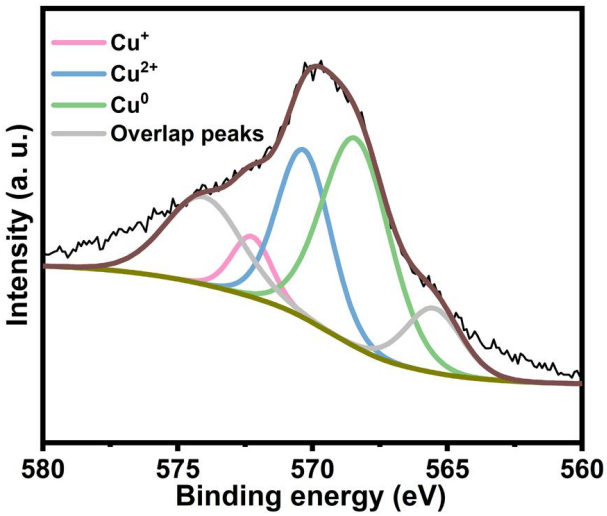

Figure S4. The Cu LMM spectrum of np-$Cu_{11}Sn_1$

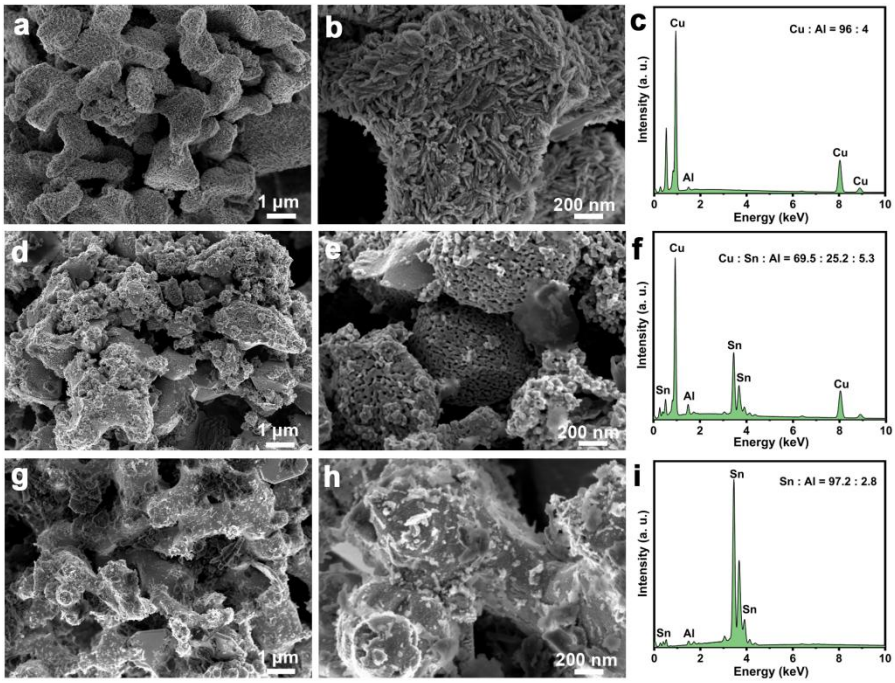

Figure S5. Typical SEM and EDS spectrum of (a-c) np-Cu, (d-f) np-Cu_1Sn_1, (g-i) np-Sn

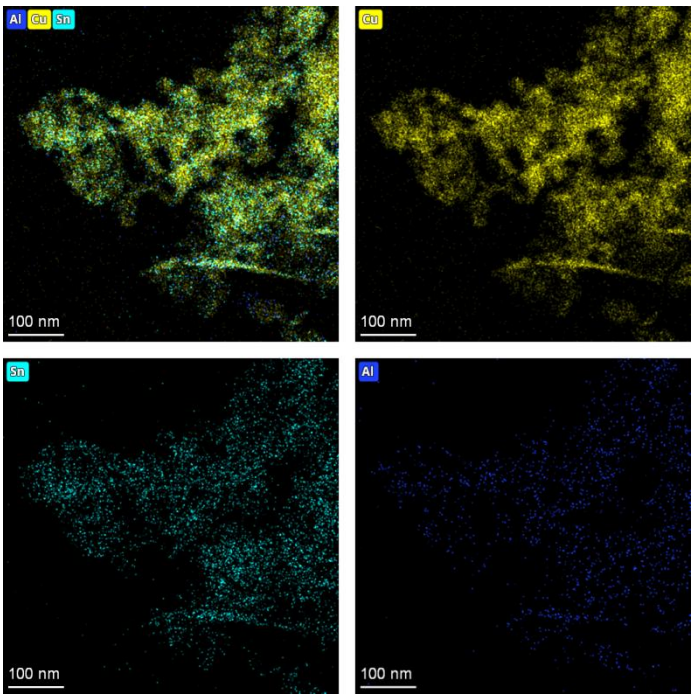

Figure S6. EDS mapping of np-$Cu_{11}Sn_1$

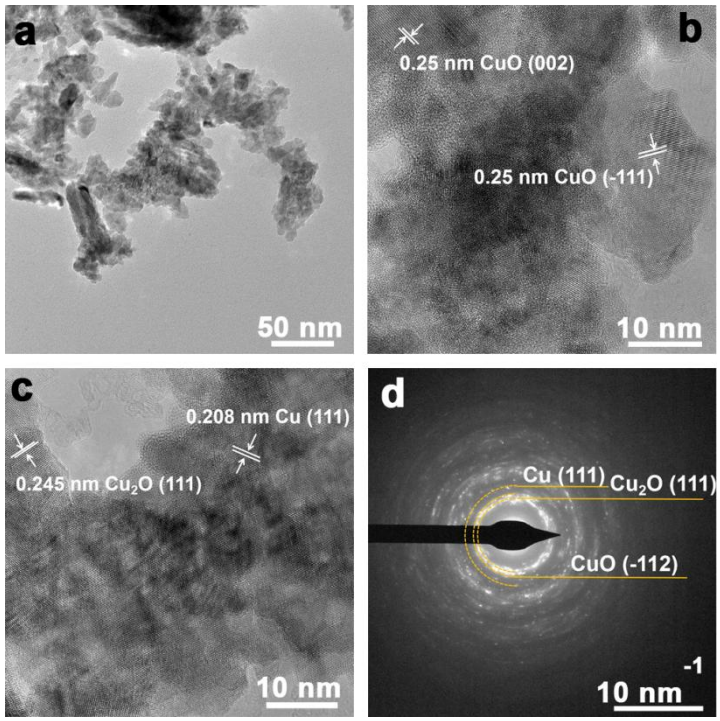

Figure S7. Typical (a) TEM, (b, c) HRTEM and (d) SAED images of np-Cu

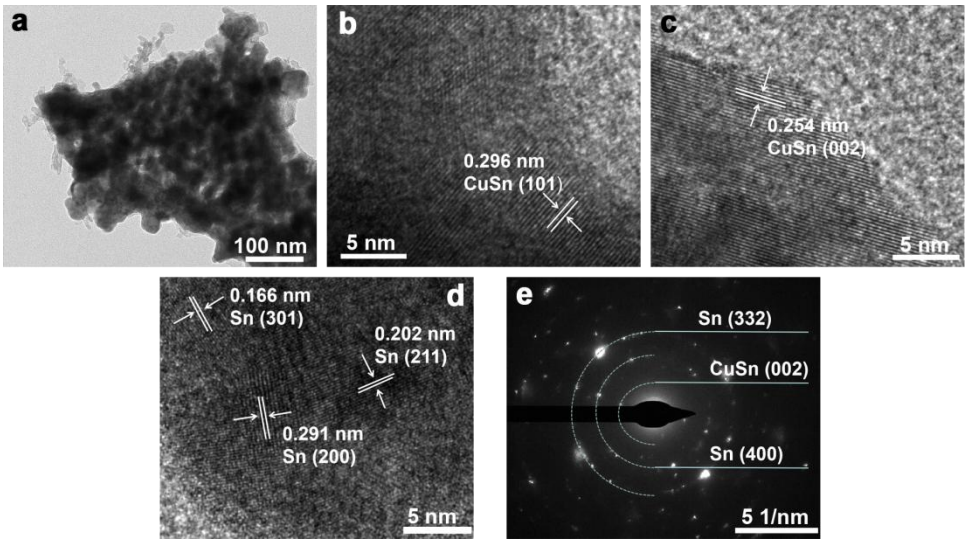

Figure S8. Typical (a) TEM, (b-d) HRTEM and (e) SAED images of np-Cu_1Sn_1

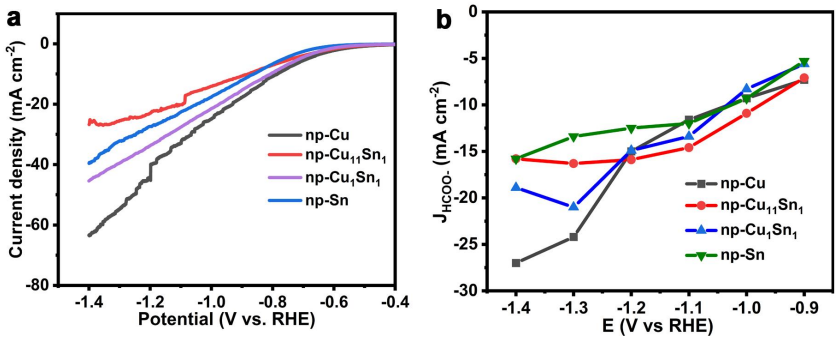

Figure S9. (a) Linear sweep voltammetry curves of np-Cu, np-$Cu_{11}Sn_1$, np-Cu_1Sn_1 and np-Sn electrodes in CO_2-saturate 0.5 M $KHCO_3$ solution with a scan rate of 10 mV s^{-1}. (b) Corresponding partial current densities for $HCOO^-$.

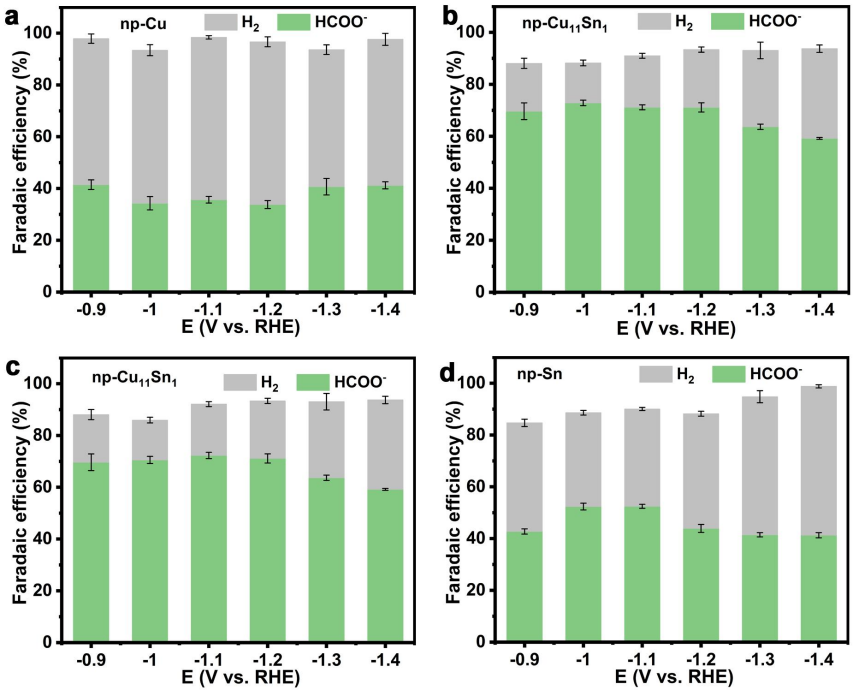

Figure S10. Potential dependence of Faradic efficiencies of np-Cu, np-$Cu_{11}Sn_1$, np-Cu_1Sn_1, np-Sn, respectively

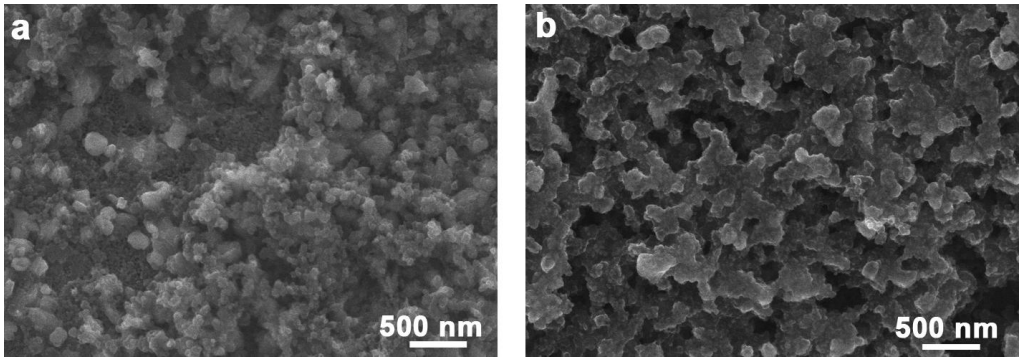

Figure S11. Surface SEM images of np-$Cu_{11}Sn_1$ (a) before and (b) after long-term stability test of electrochemical CO_2 reduction

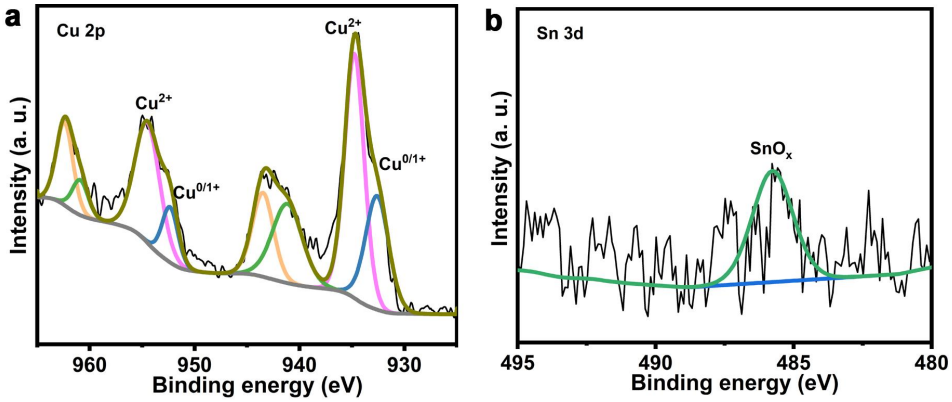

Figure S12. XPS spectrum of Cu 2p and Sn 3d for the np-$Cu_{11}Sn_1$ after stability test of electrochemical CO_2 reduction

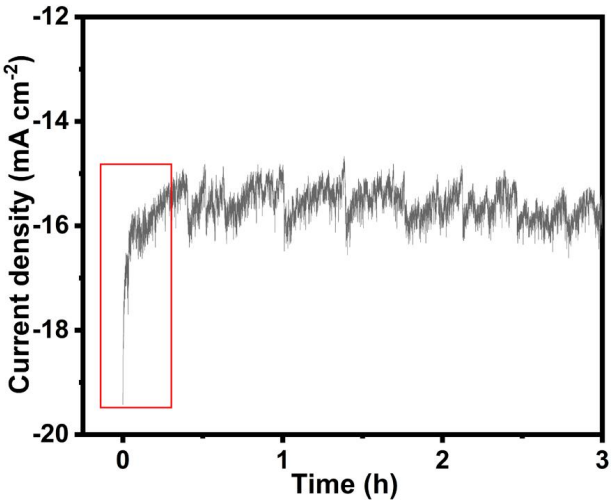

Figure S13. The long-term stability test of np-$Cu_{11}Sn_1$ at -1.0 V (vs. RHE) for 3h

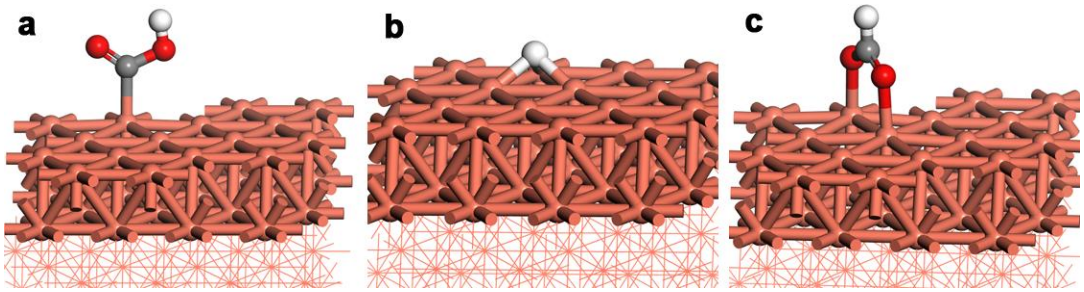

Figure S14. Adsorption models (*OCHO, *H and *COOH) on Cu(111) plane. The atoms in orange, grey, red and white represent Cu, C, O and H, respectively

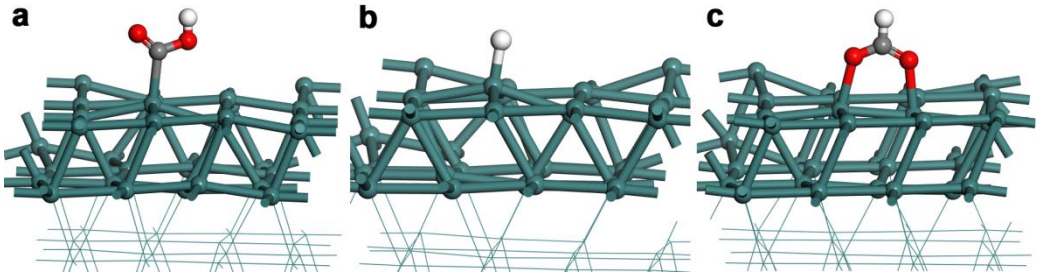

Figure S15. Adsorption models (*OCHO, *H and *COOH) on Sn(200) plane. The atoms in blackish green, grey, red and white represent Sn, C, O and H, respectively

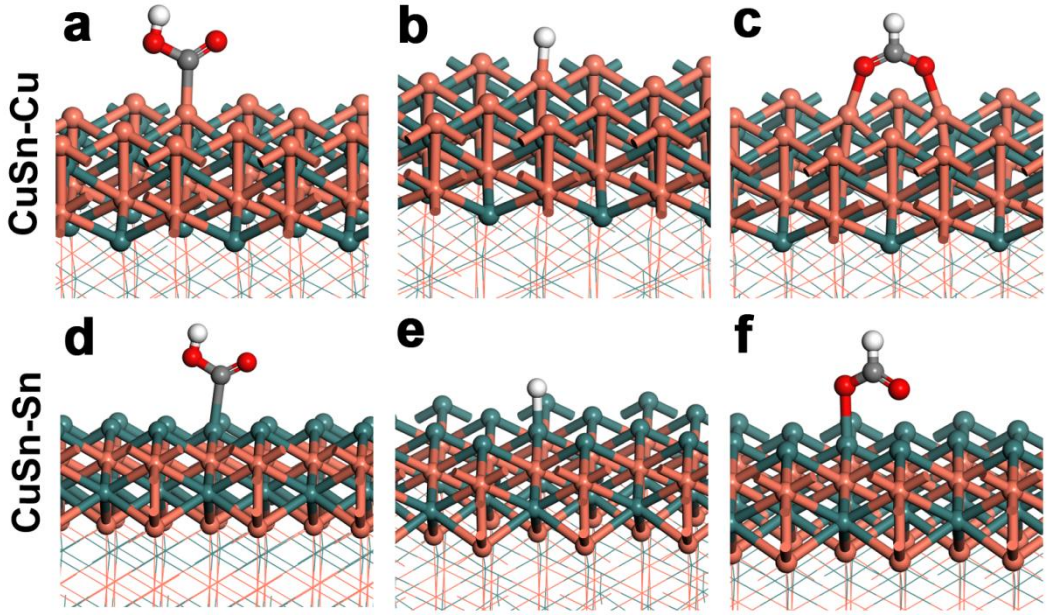

Figure S16. Adsorption models (*OCHO, *H and *COOH) on Cu and Sn site of Cu and Sn terminated CuSn(002) surface respectively. The atoms in orange, blackish green, red, grey and white represent Cu, Sn, O, C and H, respectively

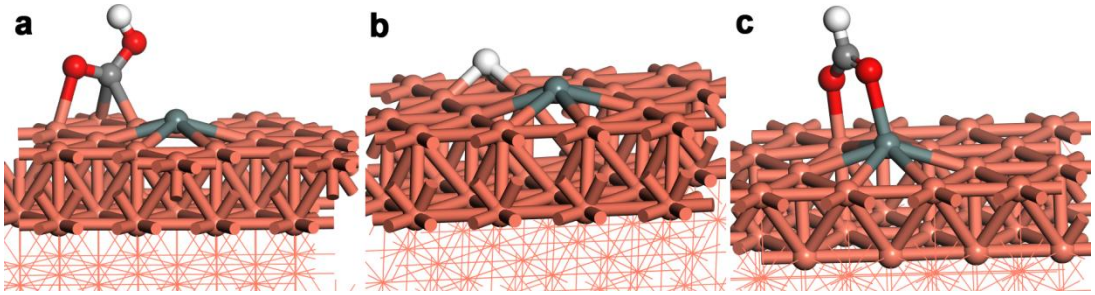

Figure S17. Adsorption models (*OCHO, *H and *COOH) on Cu(111) plane. The atoms in orange, blackish green, red, grey and white represent Cu, Sn, O, C and H, respectively

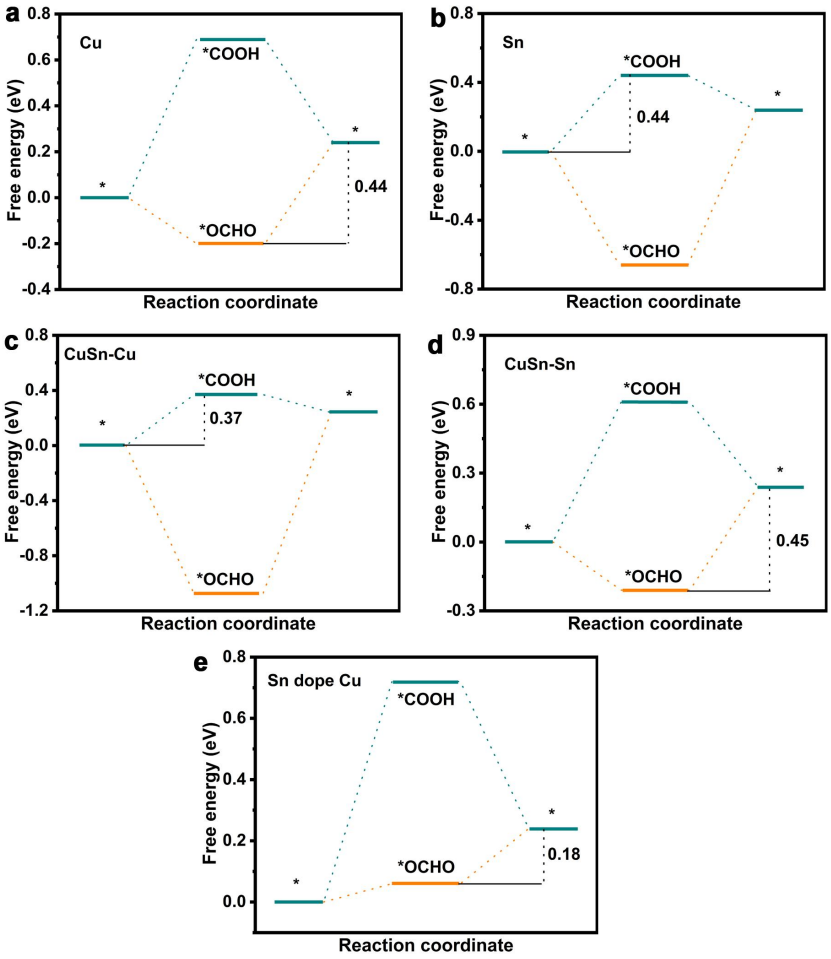

Figure S18. Comparison of calculated CO_2RR pathways to produce formic acid from *OCHO and *COOH intermediates on (a) Cu(111), (b) Sn(200), (c, d) (002) plane of CuSn-Cu and CuSn-Sn, and (e) (111) plane of Sn dope Cu.

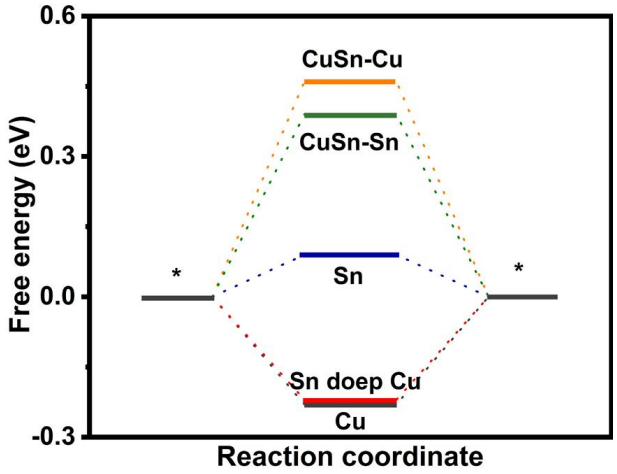

Figure S19. Reaction free-energy diagrams for the HER

Table S1 Comparison for the reported electrocatalysts toward formate formation

Catalyst	FE_{HCOO^-} (%)	Potential (V vs. RHE)	J_{HCOO^-} (mA cm^{-2})	Electrolyte	Ref.
np-$Cu_{11}Sn_1$	72.1	-1.0	10.9	0.5 M $KHCO_3$	This work
Bi-Sn-Sb	56	-1.0	N.A.	0.5 M $KHCO_3$	6
Cu_6Sn_5 NPs/CB	65.3	-0.7	7.5	0.1 M $KHCO_3$	7
Bi nanowires	74	-0.85	N.A.	0.1 M $KHCO_3$	8
Hollow Cu/Sn heterostructure	70.1	-1.0	12.6	0.1 M $KHCO_3$	9
SnO_x/Sn	70	-1.29	8.4	0.1 M $KHCO_3$	10
Cu_2O/CuS	67.6	-0.9	15.3	0.1 M $KHCO_3$	11
Cu@CuPd NWs	80	-0.3	1.9	0.5 M $KHCO_3$	12
Cu-In	70	-1.0	5.5	0.5 M $KHCO_3$	13
CuS/Cu	45	-0.6	0.4	0.1 M $KHCO_3$	14
$SnInO_x$	80	-1	5 .1	0.1 M $KHCO_3$	15

References

[1] Y. F. Wu, X. Y. Deng, H. F. Yuan, X. W. Yang, J. X. Wang, X. G. Wang, *ChemElectroChem,* 2021, **8**, 2701-2707.

[2] Z. D. Wu, J. Yu, K. Wu, J. J. Song, H. W. Gao, H. L. Shen, X. F. Xia, W. Lei, Q. L. Hao, *Appl. Surf. Sci.*, 2022, **575**, 151796.

[3] G. Kresse, J. Furthmüller, *Phys. Rev. B.*, 1996, **54**, 11169-11186.

[4] J. P. Perdew, K. Burke, M. Ernzerhof, *Phys. Rev. Lett.*, 1996, **77**, 3865-3868.

[5] S. Grimme, J. AntonPy, S. Ehrlich, H. Krieg, *J. Chem. Phys.*, 2010, **132**, 154104.

[6] B. Ávila-Bolívar, V. Montiel, J. Solla-Gullón, *ChemElectroChem*, 2022, **9**, e202200272.

[7] C. Azenha, C. Mateos-Pedrero, M. Alvarez-Guerra, A. Irabien, A. Mendes, *Electrochim. Acta*, 2020, **363**, 137207.

[8] T. Gao, X. Wen, T. Xie, N. Han, K. Sun, L. Han, H. Wang, Y. Zhang, Y. Kuang, X. Sun, *Electrochim. Acta,* 2019, **305**, 388-393.

[9] P. Wang, M. Qiao, Q. Shao, Y. Pi, X. Zhu, Y. Li, X. Huang, *Nat. Commun.,* 2018, **9**, 4933.

[10] L. Fan, Z. Xia, M. Xu, Y. Lu, Z. Li, *Adv. Funct. Mater.,* 2018, **28**, 1706289.

[11] S.W. Wang, T.Y. Kou, J.B. Varley, S.A. Akhade, S.E. Weitzner, S.E. Baker, E.B. Duoss, Y. Li, *ACS Materials Lett.,* 2020, **3**, 100-109.

[12] Y. Hou, R. Erni, R. Widmer, M. Rahaman, H. Guo, R. Fasel, P. Moreno-García, Y. Zhang, P. Broekmann, *ChemElectroChem*, 2019, **6**, 3189-3198.

[13] W. Sun, Y. Liang, C. Wang, X. Feng,W. Zhou, B. Zhang, *ChemCatChem*, 2020, **12**, 5632-5636.

[14] J.W. Lim, W.J. Dong, J.Y. Park, D.M. Hong, J.L. Lee, *ACS Appl. Mater. Interface*, 2020, **12**, 22891-22900.

[15] L.C. Pardo Pérez, D. Teschner, E. Willinger, A. Guiet, M. Driess, P. Strasser, A. Fische, *Adv. Funct. Mater.,* 2021, **31**, 2103601.